Decays of the lowest $T = 2$ states in $A = 4N$ nuclei from ^{8}Be to ^{44}Ti

S. J. Freedman,* C. A. Gagliardi, M. A. Oothoudt,† A. V. Nero,‡ R. G. H. Robertson,§ and F. J. Zutavern
Princeton University, Princeton, New Jersey 08540

E. G. Adelberger
University of Washington, Seattle, Washington 98195

A. B. McDonald
Atomic Energy of Canada Limited, AECL, Chalk River Nuclear Laboratories, Chalk River, Canada, KOJ 1JO

(Received 11 December 1978)

Branching ratios for isospin-forbidden decays have been measured for the lowest $T = 2$ levels in ^{8}Be, ^{12}C, ^{16}O, ^{24}Mg, ^{28}Si, ^{32}S, ^{36}Ar, ^{40}Ca, and ^{44}Ti. The $T = 2$ levels were populated by the isospin allowed (p,t) reaction at $E_p = 42$ or 46 MeV. Coincidences were observed between tritons detected in a quadrupole-dipole-dipole-dipole magnetic spectrometer and decay particles detected in a surface-barrier detector telescope, a time-of-flight neutron detector, or an NaI (Tl) γ-ray detector. Systematics of isospin-forbidden decay widths are discussed.

[NUCLEAR STRUCTURE ^{8}Be, ^{12}C, ^{16}O, ^{24}Mg, ^{28}Si, ^{32}S, ^{36}Ar, ^{40}Ca, ^{44}Ti; lowest $J^{\pi} = 0^{+}$, $T = 2$ level; measured isospin-forbidden particle-decay branching ratios.]

I. INTRODUCTION

The breaking of isospin symmetry in nuclei is an interesting topic in nuclear physics. The principal concern is whether or not the observed breaking can be explained by the effect of the Coulomb interaction alone. Isospin symmetry breaking is directly probed by studying isospin forbidden decays. If the interaction responsible for the decay conserves isospin then one measures the isospin mixing of the states involved. Moreover, since the final state is generally at low excitation energy in the residual nucleus, it is reasonable to attribute the observed breaking to isospin mixing in the initial state. In those circumstances where the only isospin allowed decay channels are electromagnetic, isospin forbidden particle decay usually dominates. Such systems are particularly useful since experiments can detect very small isospin admixtures. Examples can be found in light and medium weight nuclei; in particular, favorable conditions occur for the lowest $T = \frac{3}{2}$ levels in $A = 4N + 1$ nuclei and the lowest $T = 2$ levels in $A = 4N$ nuclei.

The decays of $T = \frac{3}{2}$ levels have been studied extensively and absolute decay widths have been obtained by combining the measured values of branching ratios and total widths. Relatively complete information on partial decay widths for $T_z = (N - Z)/2 = \frac{1}{2}$ and $T_z = -\frac{1}{2}$ members of $T = \frac{3}{2}$ multiplets have been assembled.[1-4] This work has revealed a number of striking and unexpected regularities. Most significant is the discovery that the variation of decay widths from nucleus to nucleus is not random but displays regular behavior. This indicates that the widths reflect basic features of nuclear charge dependence rather than the properties of "accidental" $T = \frac{1}{2}$ levels which happen to be nearly degenerate with the $T = \frac{3}{2}$ state. It is also found that a $T = \frac{3}{2}$ level with $T_z = +\frac{1}{2}$ tends to have greater reduced width[3,5,6] than the corresponding $T_z = -\frac{1}{2}$ state. This establishes that $\Delta T = 2$ and $\Delta T = 1$ mixing amplitudes are comparable,[1] at least up to $A = 25$ which is the heaviest system for which the neutron decay channel is open. The particle decays predominantly feed excited states of the residual nuclei; presumably this reflects the particle-hole structure of the isospin impurity. However, the ratios of reduced widths for decay to the various excited states are different for $T_z = \frac{1}{2}$ and $T_z = -\frac{1}{2}$, implying that the isospin admixtures include more than one nuclear configuration. Finally, there is a very surprising periodicity[4] in the proton decays of $T_z = -\frac{1}{2}$ levels to the ground states of the $A = 4N$ nuclei. The $A = 4N + 1$, $T = \frac{3}{2}$ levels with N odd have systematically larger widths than those with N even. This oscillation with a period of eight nucleons was completely unexpected and has not yet been satisfactorily explained.

Possible clues to the many unexplained regularities associated with the $T = \frac{3}{2}$ decays may be found by examining other related but very different systems, such as the $T = 2$ states of the $A = 4N$ nuclei. In contrast to the well defined decay widths for the $T = \frac{3}{2}$ levels only scattered information had been obtained for $T = 2$ states when this work was

begun. Decay branching ratios of the lowest $T=2$ states in ^{16}O had been reported by Koh *et al.*,[7] while McGrath *et al.*,[8] had measured the decay branching ratios in ^{20}Ne, ^{24}Mg, ^{28}Si, ^{32}S, and ^{40}Ca. Total widths of the $T=2$ states in ^{8}Be,[9,10] ^{16}O,[11] and ^{20}Ne (Ref. 12) had been obtained from resonance studies. Isospin allowed gamma decays of the lowest $T=2$ states in ^{20}Ne, ^{24}Mg, ^{28}Si, ^{32}P, ^{32}S, and ^{44}Ti had been observed.[12-18] It was known that proton ($\Delta T=1$ or $\Delta T=2$) and alpha ($\Delta T=2$) decays occurred with roughly equal frequencies. However, because all the resonance measurements of particle widths were confined to $A \leq 20$ it was not possible to determine if the isospin-forbidden particle widths of $T=2$ states had the same A dependence as did the $T=\frac{3}{2}$ decays, or if similar periodicities of eight nucleons occurred for the $T=2$ decays.

In this paper we report on one phase of a program to determine the systematics of the decays of the lowest $T=2$ states in $A=4N$ nuclei, namely, measurements of the branching ratios for charged particle decays in ^{8}Be, ^{12}C, ^{16}O, ^{24}Mg, ^{28}Si, ^{32}S, ^{36}Ar, ^{40}Ca, and ^{44}Ti, neutron decays in ^{8}Be, and ^{16}O and γ decays in ^{44}Ti. Relevant resonance studies have been performed at Seattle and Chalk River, and the decay widths of some of these $T=2$ states will be reported elsewhere.[19-21]

II. EXPERIMENTAL METHOD

A. Technique

The experiments were performed with beams of 42 to 46 MeV protons from the Princeton University AVF Cyclotron. The lowest $J^{\pi}=0^{+}$, $T=2$ levels of ^{8}Be, ^{12}C, ^{16}O, ^{24}Mg, ^{28}Si, ^{32}S, ^{36}Ar, ^{40}Ca, and ^{44}Ti were populated by (p,t) reactions and coincidences were observed between tritons detected at $\theta_{lab} \approx +23°$ or $+27°$ in a quadrupole-dipole-dipole-dipole (QDDD) magnetic spectrometer and various charged decay particles detected in a surface-barrier detector telescope. The detector telescope was mounted at angles of $-90°$ or $-120°$ in a 20 cm diameter scattering chamber (see Fig. 1). Various surface barrier detectors were used; the telescope was typically about 4 cm from the target. For ^{8}Be, ^{12}C, and ^{16}O, neutron decays were observed in a time-of-flight detector having a 12.5 cm diameter by 5 cm thick NE102 plastic scintillator and a 69 cm flight path. For ^{44}Ti, decay γ rays were observed in a 12.5 cm diameter by 10 cm thick NaI (Tl) detector.

After passing through the target, the beam was focused by a quadrupole doublet to a well shielded beam dump located within the concrete wall, about 7 meters from the target. This system was so effective that there was a negligible contribution

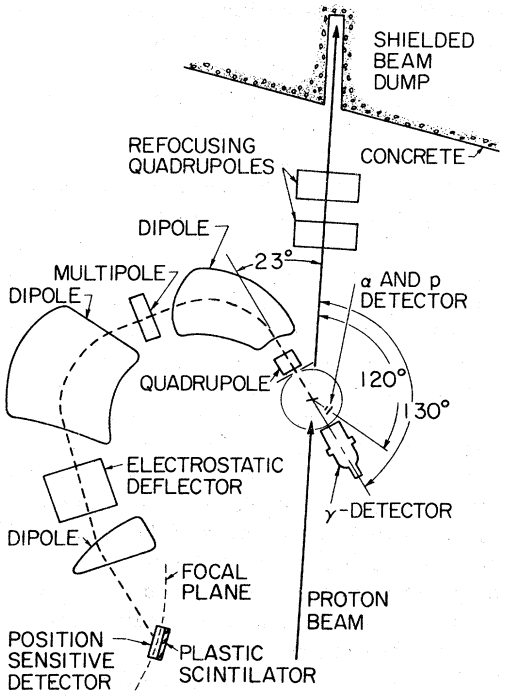

FIG. 1. Schematic diagram of the experimental apparatus.

to the counting rates in the neutron and γ-ray detectors from sources other than the target.

The focal plane detection system for the QDDD consisted of a 50 cm long resistive-wire position-sensitive proportional counter, followed by a plastic scintillator. The energy loss in the proportional counter and the total-energy signal from the scintillator were used to distinguish between tritons and other particles of similar rigidity. In addition, an electrostatic deflector between D2 and D3 reduced the background from deuterons and protons. The full solid angle of the QDDD ($\approx$14 msr) was used. In each case the various multipole elements of the spectrometer were adjusted to correct for kinematic aberration. The typical triton resolution was less than 25 keV full width at half maximum (FWHM). In most cases the resolution was limited by the finite target thickness.

Multiparameter coincidences were recorded event by event on magnetic tape by a Sigma 2 computer. Spectra corresponding to various coincident combinations were monitored on line. In addition, single parameter events corresponding to the focal plane position for identified tritons were recorded but prescaled by a factor of 10 or 100 to reduce computer dead time. By simultaneously recording singles and coincidence information, any portion of the data could be ana-

lyzed to determine branching ratios. To first order, the results are independent of beam intensity variations or target thickness changes, depending only on the overall detection efficiency of the decay-particle detectors, which was measured before and after each run.

All levels studied have $J=0$, hence the decay angular distributions are isotropic in the center of mass of the decaying nucleus and measurement at a single angle for the decay detector is sufficient to determine the branching ratios.

For the charged particle decay measurements coincidence events were composed of a time to amplitude converter (TAC) signal; energy signals from the two or three surface barrier detectors in the telescope; and the focal plane position signal for a properly identified triton. The focal plane position signal was obtained by analog division of the signals from the two ends of the resistive wire detector and triton identification was accomplished by single channel analyzers placed on the scintillator signal and on the summed signals from the two ends of the proportional counter.

The TAC was started by a signal derived from a fast beam-burst pickup, in fast coincidence with signals from the focal plane scintillator, and was stopped by a timing signal from any of the three surface barrier detectors. This choice of start signal minimized the TAC dead time because the scintillator rate (~1 kHz) was always less than the rate in the charged particle detector. The technique of using the beam burst for timing yielded a time resolution better than 1 ns (FWHM); it avoided the time slewing due to triton transit time in the QDDD ($\Delta t \approx 70$ ns). The better timing resolution provided an enhanced signal to noise ratio for charged particles and γ rays and allowed us to make high resolution time-of-flight measurements for neutrons.

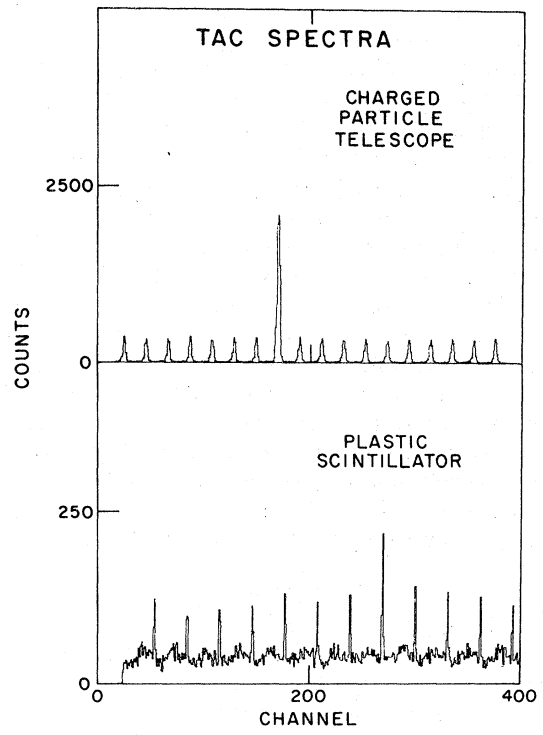

FIG. 2. Time to amplitude converter spectra for coincidences between tritons detected in the focal plane of the QDDD and (a) charged particles detected in the surface-barrier detector telescope (b) γ's and neutrons detected in the NE102 plastic scintillator.

For the γ decay measurement three parameter events consisted of triton position, TAC and γ-ray energy. For neutron decay, two parameter events consisted of triton position and TAC. A discriminator rejected events in the neutron detector due to proton recoils with energies less than 1 MeV. For the neutron flight path of 0.69 m this restricted neutron flight times to $\lesssim 50$ ns and confined real coincident events within the beam burst repetition time (50 ns). However, the large variation in flight times through the QDDD for tritons ($\Delta t \approx 70$ ns) resulted in real events occurring in two successive periods. Figure 2 shows typical TAC spectra for charged particles and neutrons. Time-of-flight spectra for neutrons were obtained by summing together the two periods containing real events after aligning them by means of the well defined prompt γ-ray produced peaks in the TAC spectrum.

B. Efficiency calibrations

To accurately determine and monitor the effective detection efficiency for charged particle decays we made measurements on a 100% particle decaying state at regular intervals during the experiments. We chose the 8.92 MeV, $J^\pi = \frac{1}{2}^-$ level of ^{13}N which was populated via the ^{14}N$(p, d)^{13}$N reaction at the same energies used in the primary measurements. The 8.92 MeV level with $\Gamma = 230$ keV decays by isospin allowed proton emission to the ground and first excited states of ^{12}C. Because of the large width it is reasonable to neglect γ emission and assume 100% proton decay for efficiency measurements. Since the spin is $\frac{1}{2}$ the proton decays will be isotropic in the center of mass. A melamine target was used for calibration of the solid target geometry and nitrogen gas was used to calibrate the gas cell geometry. Of course, the magnetic fields of the QDDD and the electronic windows on the focal plane detector had to be readjusted for calibration runs. However, branching ratios were always determined with respect to singles events in the QDDD so that procedure did not increase the uncertainty.

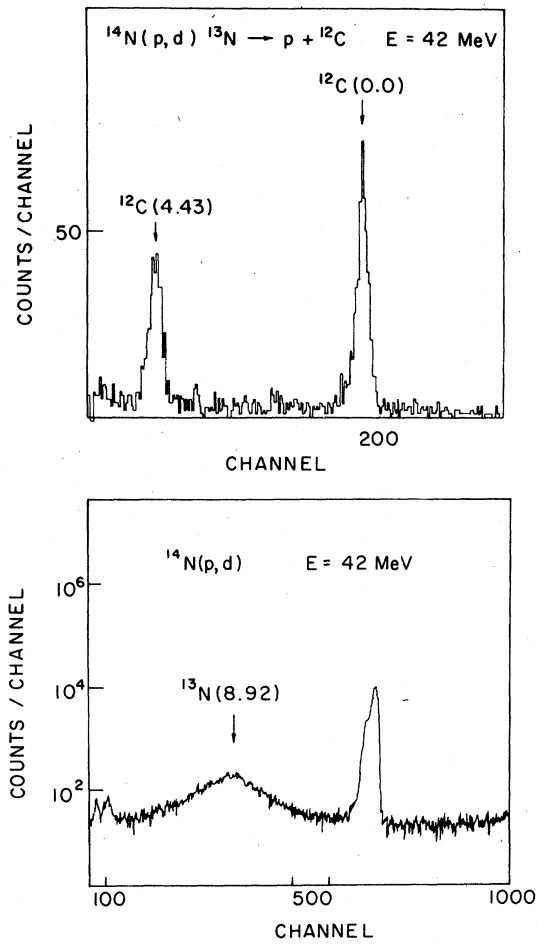

FIG. 3. (a) Focal plane position spectrum of deuterons from the ^{14}N(p,d) ^{13}N(8.92 MeV) reaction for $E_p = 42$ MeV, $\theta = 23°$. (b) Spectrum of protons from decay of ^{13}N(8.92 MeV) observed in the particle telescope at $\theta_{lab} = 120°$.

Figure 3(a) is a spectrum of deuterons from the focal plane detector; the broad, but clearly defined peak corresponding to the ^{13}N, 8.92 MeV level is evident in the figure. Figure 3(b) shows a spectrum of decay protons observed in coincidence with deuterons in the region of the 8.92 MeV level. The peaks corresponding to decays to the ground state and 4.43 MeV level of ^{12}C are well defined, and the sum of the counts in these peaks with kinematic corrections were used to define the overall detection efficiency for charged particles. In all cases, the efficiency obtained agreed within ±20% with the geometrically defined value, indicating relatively small effects due to electronic pileup and dead times. To apply a final correction, however, counting rates were monitored during actual runs and during the associated efficiency calibrations and corrections were made for the difference in dead times and pile up in the two runs. These corrections were always less than 10%. The pileup corrections were checked by studying the number of "singles" events on tape which also contained random coincidences in other ADC's.

The branching ratio for proton decay of the ^{13}N (8.92 MeV) level to ^{12}C (4.43 MeV) was also determined from the particle telescope spectra. We found $R = \Gamma_{p0}/\Gamma_{p1} = 1.6 \pm 0.1$. This result was then used to calibrate the γ-ray detector using the 4.43 MeV γ ray from the first excited state of ^{12}C. The γ-ray efficiency was extrapolated to other energies using the tables of Marion and Young[22] as discussed in Ref. 23.

The neutron detection efficiency for a similar plastic scintillator was previously measured[1] for a pulse-height threshold corresponding to a proton recoil energy of 450 keV. The higher threshold ($E_p > 1$ MeV) used in the present work was set relative to the Compton edge for γ rays from a ^{22}Na source. We used the tables of Verbinskii *et al.*[24] to define the relative light output of neutrons and γ rays. The change in detection efficiency caused by the increased threshold was also estimated from these tables.

III. RESULTS

A. ^{8}Be(27.48 MeV, $T = 2$)

The 27.483 MeV, ($J^\pi = 0^+, T = 2$) level of ^{8}Be has a large number of energetically allowed but isospin-forbidden decay channels as shown in Fig. 4. We attempted to identify as many charged particle

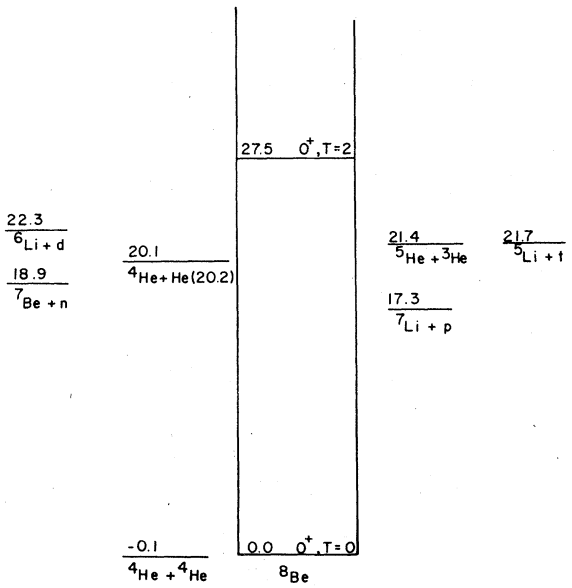

FIG. 4. Partial energy level diagram for ^{8}Be, showing possible decay modes of ^{8}Be (27.48 MeV, $T = 2$).

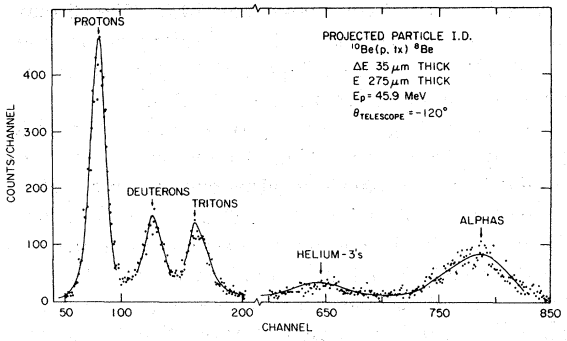

FIG. 5. Typical particle identification spectrum for the surface-barrier detector telescope.

types as possible by employing a three-element telescope consisting of 16, 35, and 1000 μm thick surface barrier detectors. (Runs ^{8}Be-2 and ^{8}Be-3). Protons and tritons penetrate the first thin E detector for energies down to $\approx$1 MeV, while ^{3}He and α particles penetrate down to laboratory energies of about 3.3 MeV. In principle these energies become the lower threshold for particle identification but in practice the threshold for unambiguous identification is somewhat higher because of noise in the second detector. The three element telescope allowed us to identify the triton and ^{3}He decays of the $T=2$ state as well as α decays to the 20.2 MeV $(0^+, 0)$ excited state of ^{4}He. The time-of-flight neutron detector was used to search for decays to ^{7}Be. An initial run (Run ^{8}Be-1) with a two-element charged particle detector telescope (35 and 275 μm) and no neutron detector provided high statistics for energetic charged particle decays.

Charged particle identification was achieved by comparing energy losses in the various elements of the telescope with known energy-range data by a "table-lookup" procedure. A typical identification spectrum is shown in Fig. 5 for the simple two element telescope. For the three-element

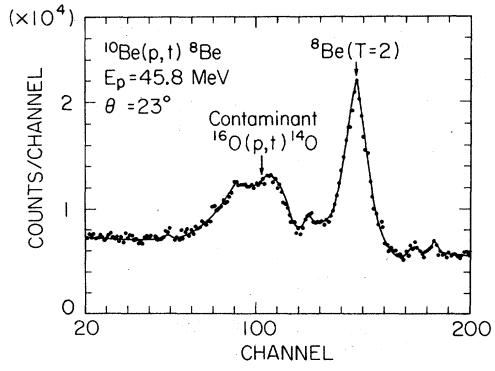

FIG. 6. Focal plane position spectrum of tritons for 45.8 MeV protons incident on the ^{10}Be O target.

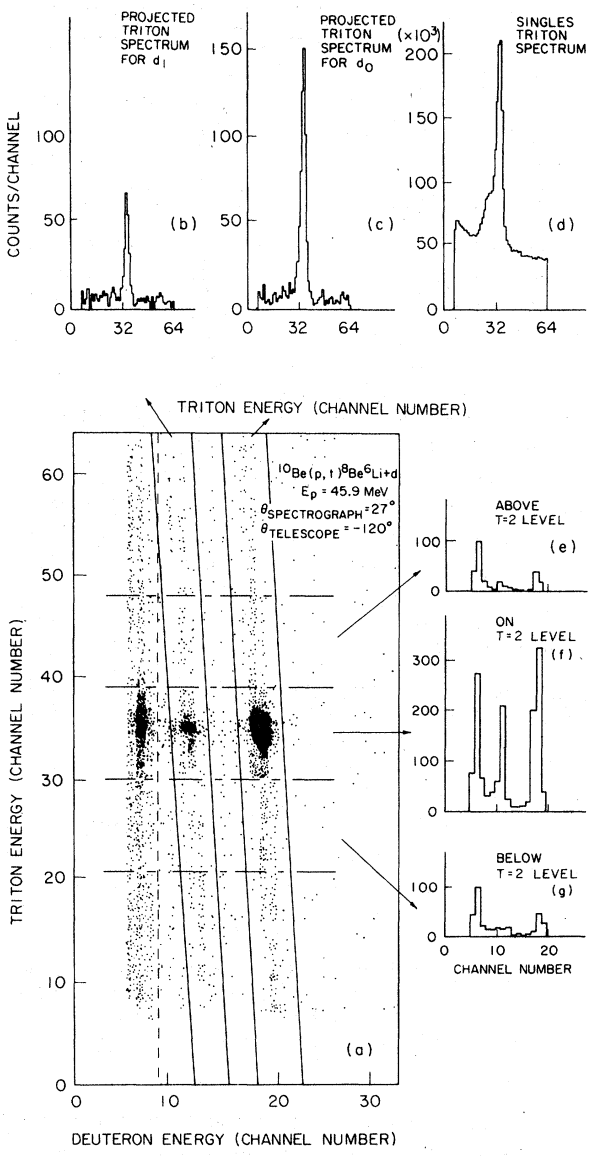

FIG. 7. (a) Spectrum of coincidences between tritons identified in the QDDD focal plane detector and deuterons identified in the surface-barrier detector telescope. The enhancements near triton channel 35 are due to the ^{8}Be (27.48 MeV, $T=2$) level. Counts to the left of the dashed line correspond to particles which stop in the front detector and cannot be identified. (b) Spectrum of t–d coincidences between the indicated solid lines corresponding to the ^{10}Be $(p,td_1)^{6}$Li(3^+_0) reaction, projected on the triton energy axis (actually focal plane position). The peak corresponds to decays of the ^{8}Be (27.48 MeV, $T=2$) level to ^{6}Li(3^+_0). (c) As in (b) but for the ^{10}Be$(p,td)^{6}$Li(1^+_0) reaction. (d) Focal plane position singles spectrum for identified tritons. Note the unresolved shoulder due to ^{16}O$(p,t)^{14}$O(7.78 MeV). (e) Spectrum of counts between the indicated dot and dash lines, projected on the deuteron energy axis. (f) As in (e) but for the region including the $T=2$ level. (g) As in (e) but for the indicated background region.

telescope, low energy particles were identified using the 16 μm ΔE detector and higher energy particles with the 35 μm ΔE detector.

The $T=2$ level was populated via the ^{10}Be$(p,t)^{8}$Be reaction using 46 MeV protons and a 200 μg/cm^2 ^{10}BeO target on a 1 mg/cm^2 Pt backing. The target was provided by Goosman; the ^{10}Be isotopic enrichment was >94%.

A portion of a typical triton singles spectrum observed in the QDDD at $\theta_{lab}=23°$ (Runs ^{8}Be-2 and ^{8}Be-3) is shown in Fig. 6. The large peak corresponding to the $T=2$ state in ^{8}Be is evident. Tritons from the reaction ^{16}O$(p,t)^{14}$O (7.78 MeV) account for the structure at lower triton energy noted in the figure. The distorted shape of the contaminant peak is due to imperfect focusing of the tritons from this reaction for the settings used in the experiment. In run ^{8}Be-1 the spectrograph angle was different ($\theta_{lab}=27°$) and the contaminant was not completely resolved [see Fig. 7(d)]. Since the ^{14}O (7.78 MeV) level decays by proton emission to ^{13}N(g.s.) the low energy decay protons from ^{8}Be($T=2$) were obscured [particularly the decay to ^{7}Li($\frac{5}{2}^-_0$, 7.467 MeV)]. In addition the error in determining branching ratios for other decays was increased significantly because of the uncertainty in determining the singles yield. The results in Table I are obtained by a weighted average of Run ^{8}Be-1, ^{8}Be-2, and ^{8}Be-3 for all decay channels where decay particle identification was unambiguous. Otherwise only the results of ^{8}Be-2 and ^{8}Be-3 were included. In Runs ^{8}Be-1 and ^{8}Be-2 the telescope was at $-120°$ and in Run ^{8}Be-3 at $-90°$.

Figure 7(a) shows a two dimensional histogram of events corresponding to coincidences between tritons in the QDDD and decay particles in the deutron identification peak (see Fig. 5 from Run ^{8}Be-1). The axes of the plot correspond to triton momentum (position in the focal plane of the QDDD) and deuteron energy (as measured by the particle telescope).

The dashed verticle line indicates the minimum deuteron energy which passes through the 51 μm detector. Counts below this threshold are from particles which stop in this detector and could arise from low energy d, α, ^{3}He, or triton decay particles. In subsequent figures such unidentified decay particles will not be plotted except for a few cases as noted in the figure captions. The enhancements seen in Fig. 7 cluster along kinematic lines determined by energy and momentum conservation in the three body final state. The particularly significant enhancements around channel 35 (triton energy) correspond to decays of ^{8}Be($T=2$) to

TABLE I. Decay properties of the 27.49 MeV, $J^\pi=0^+$, $T=2$ level of ^{8}Be.

Channel		Branching ratio (%)	Γ_i(eV) Experiment [a]	Theory [b]	γ^2/γ^2_{WL} ($\times10^{-6}$)
α	$+^{4}$He(0^+_0)	0.2 ± 0.4	11 ± 22	200	0.5 ± 1.0
	$+^{4}$He(0^+_1)	10.6 ± 1.8	583 ± 99		54 ± 9
p	$+^{7}$Li$(\frac{3}{2}^-_0)$	0.6 ± 0.6	33 ± 33	200	1.8 ± 1.8
	$(\frac{1}{2}^-_0)$	2.6 ± 0.6	143 ± 33	100	7.8 ± 1.8
	$(\frac{7}{2}^-_0)$	3.0 ± 1.5	165 ± 83		122 ± 61
	$(\frac{5}{2}^-_0)$	3.2 ± 2.0	176 ± 110		530 ± 330
	$(\frac{7}{2}^-_1)$	<4	<220		<1571
n	$+^{7}$Be				
	$(\frac{3}{2}^-_0+\frac{1}{2}^-_0)$	14 ± 7	770 ± 470		≈43 ± 26
	$(\frac{7}{2}^-_0)$	16 ± 8	880 ± 540		5000 ± 2500
	$(\frac{5}{2}^-_0+\frac{5}{2}^-_1)$	24 ± 12	1320 ± 805		
d	$+^{6}$Li(1^+_0)	28 ± 4	1540 ± 220	3800	143 ± 20
	(3^+_0)	9 ± 2	495 ± 110	300	182 ± 41
t	$+^{5}$Li	16 ± 4	880 ± 220	40	≈100
^{3}He	$+^{5}$He	9 ± 2	495 ± 110	30	≈50
$\gamma(M1)$	$+^{8}$Be(0^+_0)		21.9 ± 3.9	16	
Γ_{total}			5500 ± 2000	4900	

[a] $\Gamma=5.5\pm2$ keV, Ref. 10.

[b] Reference 37.

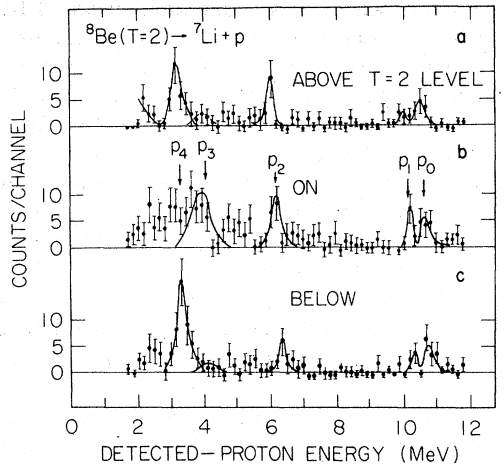

FIG. 8. Spectra of protons identified in the surface-barrier detector telescope in coincidence with tritons in three regions of the focal plane as indicated in Fig. 7(e)–(g).

^{6}Li(1^+_0, g.s.) and ^{6}Li(3^+_0, 2.185 MeV). Projections of the two dimensional spectra onto the triton momentum and the deuteron energy axes are shown in Figs. 7(b)–7(g).

Spectra projected onto the triton energy axis were ordinarily used to determine branching ratios (in some cases the other projection was used to help subtract overlapping background). The backgrounds subtracted in each case were determined by linear interpolation between the background levels on either side of the peaks. Branching ratios were calculated from the ratio of counts in the "$T=2$" peaks in the coincident and singles triton spectra, with corrections applied for overall detection efficiency, including pileup dead time effects, and for solid angle transformation from laboratory to center-of-mass frames.

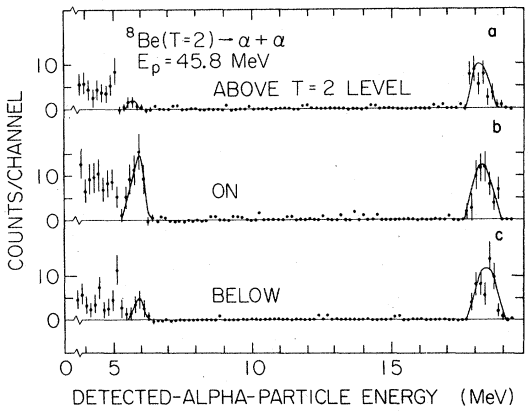

FIG. 9. α particle decay spectra projected on the decay particle detector axis as in Fig. 7 (e)–(g).

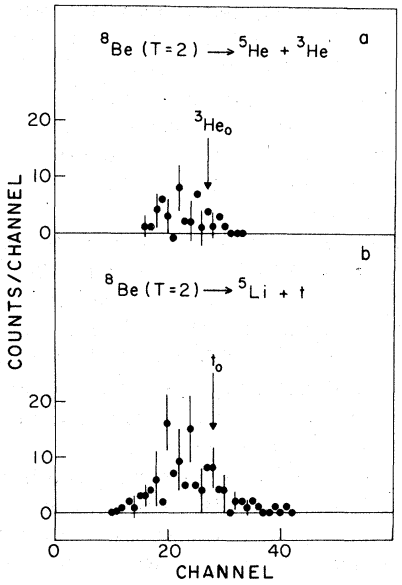

FIG. 10. ^{3}He (a) and t (b) decay spectra corresponding to ^{8}Be ($T=2$), projected on the decay particle detector axis with background spectra subtracted.

Figures 7(e)–7(g) show the spectra of deuteron decay particles projected onto the decay energy axis. The decay properties of the $T=2$ state are clearly dominated by the deuteron decay to the ground state and first excited state of ^{6}Li.

Similar projections on the decay axis for runs ^{8}Be-2 and ^{8}Be-3 are shown for decay protons in Fig. 8(a)–7(c). Here one can observe significant

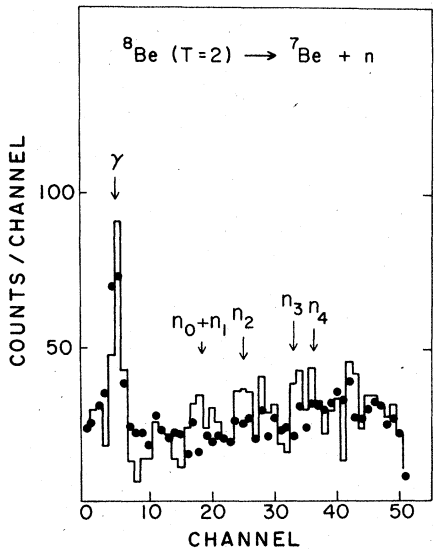

FIG. 11. Time-of-flight neutron spectrum corresponding to the ^{8}Be ($T=2$) peak after background subtraction (histogram). The filled circles correspond to a normalized random spectrum (see text).

decay for regions on either side of the $T=2$ peak. The large peak at about 3.2 MeV in Fig. 8(c) arises from proton decay of the ^{14}O(7.78 MeV) level, clearly observable in the triton spectrum of Fig. 6.

Figure 9(a)–(c) shows similar projections for α particle decay. Whereas little or no enhancement in the region of the $T=2$ peak is observed for decay to the ground state of ^{4}He ($E_\alpha \approx 18.5$ MeV), there is clear evidence for decay to the 20.5 MeV, $J^\pi = 0^+$ first excited state ($E_\alpha \approx 6$ MeV).

Projected decay spectra for ^{3}He and t decay, corresponding to the $T=2$ peak after subtraction of a kinematically corrected background spectrum, are shown in Fig. 10(a) and 10(b), respectively. Broad continua are observed, expected for the unbound residual nuclei ^{5}He and ^{5}Li and branching ratios were evaluated for the total number of counts above threshold.

The time-of-flight neutron spectrum corresponding to the $T=2$ peak after background subtraction is shown as a histogram in Fig. 11, together with the normalized random spectrum (filled circles) corresponding to the average of seven beam repetition periods. The large peak at the left corresponds to prompt γ rays from the target and was used to align the random spectra for averaging. The time scale in ns/m was derived from the known beam repetition frequency and the target to detector distance of 0.66 m. The random coincidence rate was sufficiently large (due to the thick Pt backing) that the statistical accuracy of the neutron branching ratios was very poor, but small net excess of counts were observed for decays to the channels indicated.

Final branching ratios were obtained as a weighted average from all the runs in which the particular decay particles were unambiguously identified and are listed in Table I. These are the first branching ratio measurements for the 27.49 MeV $T=2$ state. This state has been observed as a resonance in ^{6}Li(d,p_1) and ^{6}Li(d,α) by Black *et al.*,[9] in ^{4}He(α,p) and ^{4}He(α,d) by Hinterberger *et al.*[25] and in ^{6}Li(d,γ) by Noé *et al.*[10] These different experiments have yielded inconsistent values for $\Gamma_{c.m.}$: (10 ± 3) keV, (14.7 ± 4.0) keV, and (5.5 ± 2.0) keV, respectively. We have adopted the value 5.5 ± 2.0 keV given in Ref. 10. Although the charged particle resonance studies have indicated finite decay widths for the p_1, d_0, and α_0 channels, quantitative partial widths were not obtained previously due to the complications introduced by nonzero channel spins. Partial widths in the c.m. system, obtained by combining our branching ratios with $\Gamma_{c.m.}$ from Ref. 10 are listed in Table I, along with the corresponding reduced widths in single particle units, $\theta_i^2 = \gamma_i^2/\gamma_{WL}^2 \equiv \Gamma_i/2P\gamma_{WL}^2$ where Γ_i is the particle decay width, P is the Coulomb penetrability and $\gamma_{WL}^2 = 2\hbar^2/\mu R$ is the Wigner limit width. In all cases in this paper, P and γ_{WL}^2 were calculated using a radius $R = 1.4 \times (A_1^{1/3} + A_2^{1/3})$ fm.

The radiative width Γ_{M1} is obtained by combining the value $\Gamma_{M1}\Gamma_{d_0}/\Gamma = (6.12\pm0.64)$ eV from Ref. 10 with our value for Γ_{d_0}/Γ.

B. ^{12}C (27.6 MeV, $T=2$)

The 27.6 MeV $(0^+, 2)$ level of ^{12}C was populated in the ^{14}C$(p,t)^{12}$C reaction using 46 MeV protons. The 300 μg/cm^2 ^{14}C target on a 1 mg/cm^2 Au

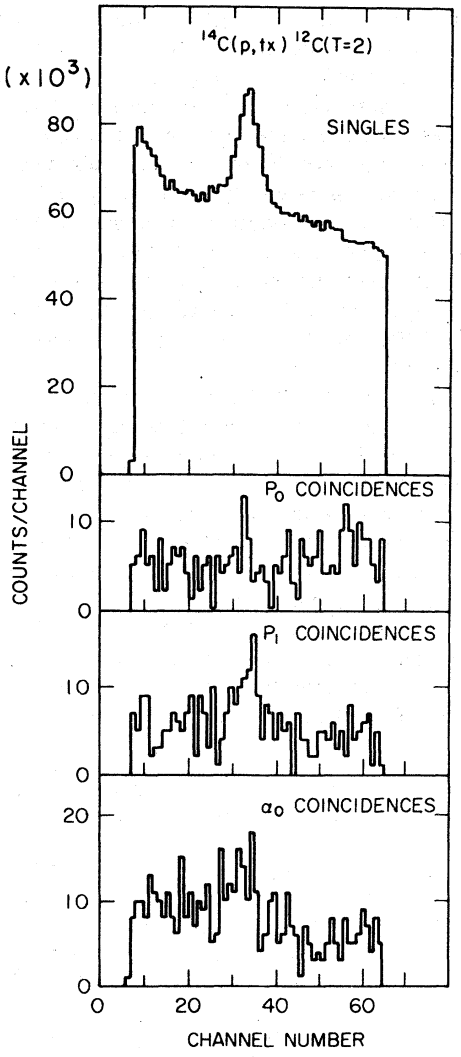

FIG. 12. QDDD focal plane position spectra of tritons from the ^{14}C$(p,t)^{12}$C reaction at $E_p = 46$ MeV for (a) singles, (b) coincidences with proton decays to ^{11}B(0.0 MeV), (c) coincidences with proton decays to ^{11}B(2.12 MeV), (d) coincidences with alpha decays to ^{8}Be (0.0 MeV). The peak corresponds to the 27.6 MeV, $T=2$ level of ^{12}C.

backing was made by cracking acetylene (enriched to ≈94% ^{14}C).

The low cross section for the $^{12}C(T=2)$ level (~10 μb/sr) and the large background (due in part to reactions with the thick gold backing) made it difficult to obtain good statistical accuracy for branching ratios. The high random coincidence rate precluded any measurement of neutron branching ratios. Figure 12 shows the singles triton spectrum for $\theta_{lab}=27°$ as well as the corresponding real coincidence triton spectra associated with proton decays to ^{11}B(g.s.) and ^{11}B(2.12 MeV), and α decays to ^{8}Be(g.s.). These data were obtained with the two-element telescope described above at −120° to the beam (Run ^{12}C-1). Additional data were taken with the three element telescope at −90° which allowed us to measure the branching ratio for deuteron decays to ^{10}B(g.s.). The results for these two runs are combined in Table II.

Figure 13 shows the background subtracted real coincidence α particle spectra for Runs ^{12}C-1 and ^{12}C-2. It was constructed by subtracting projected spectra above and below the $T=2$ peak from the spectrum on resonance. A peak is observable corresponding to decays to the ground state of ^{8}Be, but for higher excitation energies a continuum is observed.

The measured branching ratios are listed in Table II, including an entry labeled "continuum," associated with the net counts below channel 40 in Fig. 13. The latter branching ratio was calculated as though the decay proceeded sequentially through excited states of ^{8}Be and only the α particle from the primary decay was detected. Since a significant proportion of this yield may arise from $^{12}C(T=2)\rightarrow 3\alpha$ directly, with the possibility of detecting any of the three alphas, the branching ratio in this channel may be smaller by up to a factor of 3. The present results are in reasonable agreement with and more precise than the previous measurement by Ashery *et al.*[26]

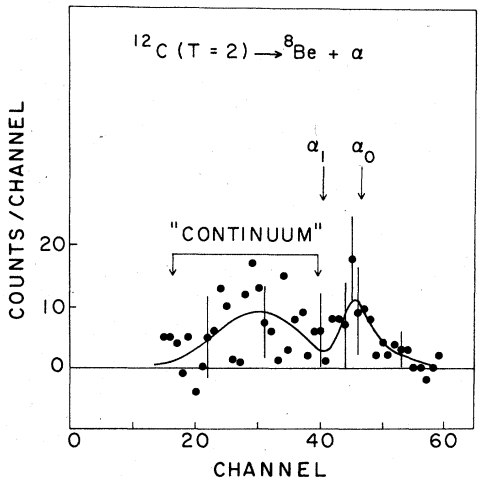

FIG. 13. Surface-barrier detector telescope energy spectrum for alpha particles in coincidence with tritons from $^{14}C(p,t)^{12}C$(27.6 MeV, $T=2$). An average background spectrum has been subtracted.

The 27.6 MeV, $T=2$ level of ^{12}C has been sought extensively as an isospin-forbidden resonance in the $^{11}B(p,\gamma\gamma)$, $^{10}B(d,p)$, $^{10}B(d,\alpha)$, $^{10}B(d,\gamma\gamma)$, and $^{9}Be(^{3}He,\gamma\gamma)$ reactions.[27-30] A tentative identification of the level as a resonance in the $^{9}Be(^{3}He,\gamma\gamma)$ reaction[28] was not verified in two other searches in the same channel.[29,30] Searches in the other channels found no resonance. The present branching ratio measurements indicate why these measurements have not been successful. The $T=2$ level decays primarily via α particles or protons to excited states, with very small ground state branches for protons or deuterons. In our experiment ^{3}He particles from a possible decay branch to ^{9}Be are too low in energy (~1 MeV) to have been

TABLE II. Decay properties of the 27.6 MeV, $J^{\pi}=0^{+}$, $T=2$ level of ^{12}C.

Channel	Branching ratio (%) Present work	Ref. 26	Γ_i [a] (eV)	$\gamma^2/\gamma^2_{W_L}$ ($\times 10^{-6}$) [a]
$\alpha + {}^{8}Be(0^{+}_{0})$	10.5 ± 3.0	<10	<4050	<285
+ "Continuum"	9.1 ± 3.5		<3750	•••
$p + {}^{11}B(\frac{3}{2}^{-}_{0})$	3.0 ± 2.2		<1650	<91
$+ {}^{11}B(\frac{1}{2}^{-}_{0})$	8.0 ± 2.3	$\Sigma = 30 \pm 10$	<3090	<196
$+ {}^{11}B(\frac{5}{2}^{-}_{0})$	0 ± 3.3		<990	<316
$+ {}^{11}B(\frac{3}{2}^{-}_{1})$	8.4 ± 3.2		<3450	<290
$+ {}^{11}B(\frac{7}{2}^{-}_{0} + \frac{1}{2}^{+}_{0})$	8 ± 5		<3900	•••
$d + {}^{10}B(3^{+}_{0})$	2.8 ± 2.0		<1440	<973

[a] Upper limit based on $\Gamma < 30$ keV (Ref. 31).

identified.

A recent study of the $T=2$ state via the $^{14}C(p,t)$ reaction[31] has yielded an upper limit of 30 keV for the width of the level. This result was used to define upper limits for reduced widths listed in Table II.

C. ^{16}O (22.72 MeV, $T=2$)

The lowest $T=2$ level in ^{16}O was populated by the $^{18}O(p,t)^{16}O$ reaction with 42.4 MeV protons incident upon a target consisting of 200 $\mu g/cm^2$ of WO_3 (enriched to >90% in ^{18}O) on a 10 $\mu g/cm^2$ carbon backing. The spectrum of tritons observed in the focal plane of the QDDD spectrometer at $\theta_{lab} = +23°$ is shown in Fig. 14(a). The $T=2$ level is clearly observed with an energy resolution of 25 keV FWHM. Decay particles were observed at laboratory angles of $-90°$ and $-120°$ in a three-element detector telescope consisting of 16-, 51-, and 1000-μm surface-barrier detectors. Figures 14(b) and 14(c) show the spectra of α particles and protons observed in coincidence with tritons

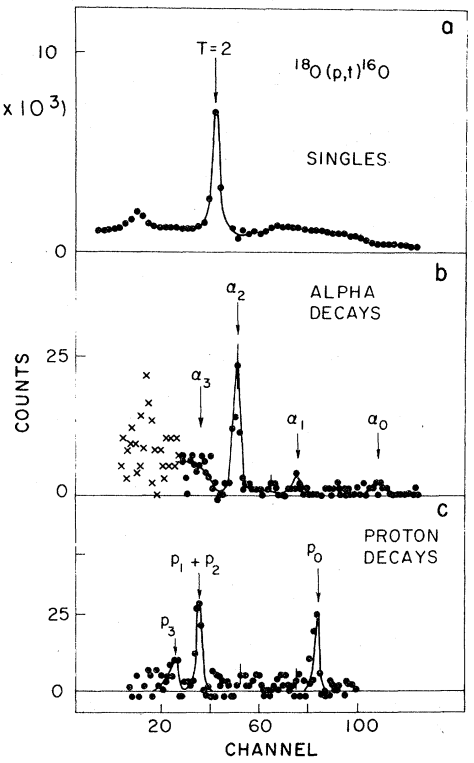

FIG. 14. (a) A QDDD focal plane position spectrum for tritons from the $^{18}O(p,t)^{16}O$ reaction for $E_p = 42.4$ MeV. (b) Surface-barrier detector telescope energy spectrum of α particles in coincidence with tritons in the $T=2$ peak of (a). The crosses indicate events wherein the particles stopped in the front detector and could not be unambiguously identified as α particles. (c) As in (b) but for proton decays.

associated with the production of the $T=2$ level. Clear indication of decay strength is seen for both particle types. Events in the α particle spectrum below about 4 MeV (plotted as crosses) correspond to particles which stop in the 16-μm front detector and include some carbon, nitrogen or oxygen ions from light particle decays. Figure 15 shows time-of-flight spectra for real (solid line) and random (dots) coincidence between tritons in the peak associated with the $T=2$ level and neutrons or γ rays detected in the plastic scintillator. The real spectrum is the sum of two rf periods and the random spectrum is the normalized sum of eight rf periods. Statistically significant peaks are observed in the expected regions for neutrons decaying to the first two excited states of ^{15}O and for γ rays (probably from gamma decay of states populated by particle decays).

Branching ratios from the present work are compared with those from previous studies in Table III. There is excellent agreement between the present work and the results of Nero *et al.*,[11] but some discrepancies exist in comparison with the results of Koh *et al.*,[7] particularly for the proton branching ratios. This may be due to the much poorer energy resolution in Ref. 7 (400 keV FWHM). Recently this $T=2$ level was sought as a resonance in high resolution studies of the $^{15}N(p,p)$ reaction and not observed,[32] in agreement with the small branching ratio measured in the present work.

A total width of 12.5 ± 3.5 keV was obtained for this level by Nero *et al.*[11] and confirmed by McDonald *et al.*[32] using the $^{12}C(\alpha,\alpha_2)$ reaction.

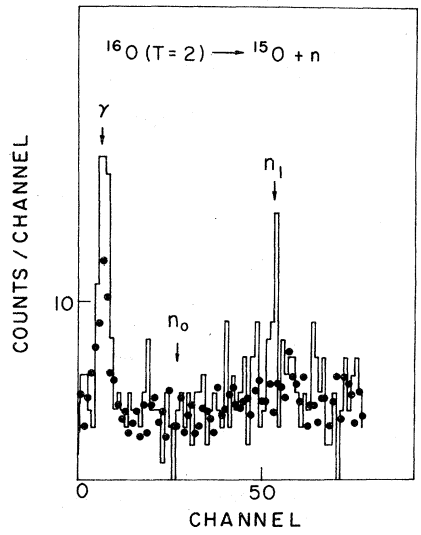

FIG. 15. Time-of-flight neutron spectrum corresponding to the $^{16}O(T=2)$ peak after background subtraction (histogram). The filled circles correspond to a normalized random spectrum (see text).

TABLE III. Decay properties of the 22.72 MeV, $J^\pi=0^+$, $T=2$ level of ^{16}O.

Channel	Branching ratio (%) Present work	Ref. a	Ref. b	Γ_i (eV) [c]	γ^2/γ^2_{WL} ($\times10^{-6}$)
$\alpha+^{12}C(0^+_0)$	1.6 ± 0.7	2.0 ± 0.6	1 ± 4	190 ± 100	19 ± 10
$+^{12}C(2^+_0)$	1.9 ± 0.7		0 ± 3	230 ± 110	30 ± 14
$+^{12}C(0^+_1)$	14 ± 2	13 ± 5		1680 ± 550	260 ± 85
$p+^{15}N(\frac{1}{2}^-_0)$	7 ± 2	≥6	25 ± 6	840 ± 343	55 ± 22
$+^{15}N(\frac{5}{2}^+_0+\frac{1}{2}^+_0)$	11 ± 2		21 ± 5	1320 ± 454	···
$+^{15}N(\frac{3}{2}^-_0)$	5 ± 2		14 ± 5	600 ± 300	87 ± 44
$n+^{15}O(\frac{1}{2}^-_0)$	<15			<2325	<171
$+^{15}O(\frac{1}{2}^+_0+\frac{5}{2}^+_0)$	23 ± 15			2760 ± 1970	···

[a] Reference 11.
[b] Reference 7.
[c] $\Gamma=12\pm3.5$ keV (Refs. 11 and 32).

D. ^{24}Mg (15.43 MeV, $T=2$)

Figure 16 shows the spectrum of tritons at $\theta_{lab}=23°$ from the ^{26}Mg$(p,t)^{24}$Mg reaction for 42.4 MeV protons incident on a 200 μg/cm^2 ^{26}Mg (enriched to >95%) layer on a 10 μgm/cm^2 carbon backing. Also shown are the spectra of protons and α particles corresponding to particle decays of the $T=2$ state to energy levels of ^{23}Na and ^{20}Ne. The decay particles were detected in a 51-μm–1000-μm particle detector telescope at $-120°$. The charged particle decay branching ratios are summarized in Table IV. The branching ratios for α decay are in reasonable agreement with the previous results of McGrath *et al.*,[8] but there is some discrepancy for the proton branches. Partial widths and reduced widths for the decays have been deduced by combining our results with the recently measured $\Gamma=500\pm200$ eV obtained by the ^{23}Na(p,p) (Ref.19) and ^{23}Na(p,γ) (Ref. 20) reactions. Previous measurements by the ^{23}Na(p,γ) reaction[14,33] have defined the gamma decay properties of the level.

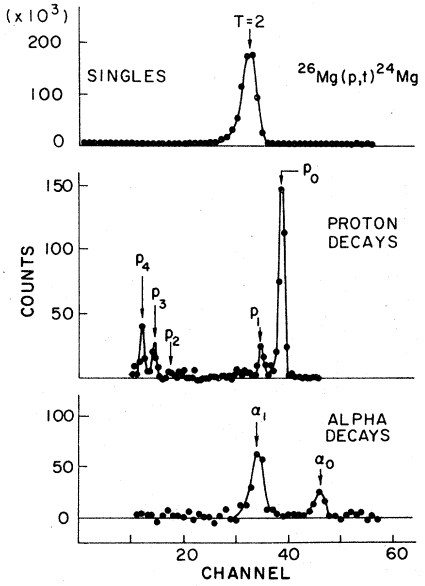

FIG. 16. Singles triton spectrum and coincidences spectra for proton and alpha decays of the ^{24}Mg (15.43 MeV, $T=2$) level (see caption of Fig. 14).

E. ^{28}Si (15.22 MeV, $T=2$)

The ^{28}Si (15.22 MeV, $J^\pi=0^+$, $T=2$) level was produced with 42 MeV protons incident on a 200 μg/cm^2 SiO_2 target enriched to >90% in ^{30}Si. Figure 17 shows the singles triton spectrum observed in the QDDD spectrometer at $\theta_{lab}=27°$ as well as spectra of protons and α particles corresponding to the various decay modes of the $T=2$ level. The decay particles were detected in a 50- and 1000-μm particle detector telescope at $-120°$. The resultant branching ratios shown in Table IV are in excellent agreement with those of McGrath *et al.*,[8] but have better precision. The $T=2$ level in ^{28}Si was previously observed as a resonance in the ^{24}Mg(α,γ) reaction,[27,15] and an upper limit of 2 keV was obtained for the total width. The observation of a resonance in the gamma yield from ^{24}Mg(2^+_0) was used in the latter work[15] to infer $\Gamma_{\alpha_1}=35\pm20$ eV, which may be combined with the present branching ratio measurement to yield $\Gamma_{\alpha_0}=301\pm190$ eV, in agreement with a recent precise measurement $\Gamma_{\alpha_0}=222\pm25$ eV, by the ^{24}Mg(α,α) reaction.[21]

TABLE IV. Particle decay properties of lowest $T=2$ levels ($J^\pi=0^+$).

Channel	Branching ratio (%) Present work	Ref. 8	Γ_i(eV)	γ^2/γ^2_{WL} ($\times10^{-6}$)
^{24}Mg(1543 MeV)	($\Gamma=435\pm135$ eV [a])			
$\alpha+^{20}$Ne(0^+_0)	6 ±1.3	3±3	30± 14	9.4±4.4
^{20}Ne(2^+_1)	18 ±2	22±4	90± 37	92±38
$p+^{23}$Na($\frac{3}{2}^+_0$)	49 ±6	71±7	245±103	135±57
^{23}Na($\frac{5}{2}^+_0$)	7 ±2	1±4	35± 17	27±13
^{23}Na($\frac{7}{2}^+_0$)	1 ±1		5± 5	15 000±15 000
^{23}Na($\frac{1}{2}^+_0$)	4.6±1		23± 14	31±19
^{23}Na($\frac{1}{2}^-_0+\frac{9}{2}^+_0$)	7 ±1		35± 15	···
^{28}Si(15.22 MeV)	($\Gamma_{\alpha0}=222\pm25$ eV [b])			
$\alpha+^{24}$Mg(0^+_0)	69 ±6	72±8	222± 25	135±15
$+^{24}$Mg(2^+_0)	8 ±2	8±4	26± 8	135±41
$p+^{27}$Al($\frac{5}{2}^+_0$)	3.5±2	4±8	11± 6	7.9±4.3
$+^{27}$Al($\frac{1}{2}^+_0+\frac{3}{2}^+_0$)	<2	4±5	<7	···
$+^{27}$Al(2.2 to 2.9 MeV)	<16		<59	···
^{32}S(12.05 MeV)	($\Gamma<170$ eV) [c]			
$\alpha+^{28}$Si(0^+_0)	4 ±4	18±7	<14	<16
$+^{28}$Si(2^+_1)	<2	11±5	<3.4	<283
$p+^{31}$P($\frac{1}{2}^+_0$)	100 ±13	86±17	<192	<60
$+^{31}$P($\frac{3}{2}^+_0$)	4 ±4		<14	<194
^{44}Ti(9.34 MeV)	($\Gamma=1.10\pm0.28$ eV) [d]			
$\alpha+^{40}$Ca(0^+_0)	32 ±5	···	0.35±0.07	57±11
$p+^{43}$Sc($\frac{7}{2}^-_0$)	<4	···	<0.055	···
$\gamma+^{44}$Ti(1^+)	54 ±11		0.75±0.19	

[a] References 19 and 20.
[b] Reference 21.
[c] Reference 17 for $\Gamma_p/\Gamma=100\%$.
[d] Reference 23.

F. ^{32}S (12.05 MeV, $T=2$)

The spectrum of tritons at 27° from the ^{34}S(p,t)^{32}S reaction at $E_p=42$ MeV is shown in Fig. 18(a). The target consisted of 200 μg/cm^2 of ^{34}S, isotopically enriched to greater than 95%, deposited on a 20 μg/cm^2 carbon foil and covered with a second 20 μg/cm^2 carbon foil. The only significant decay branch observed was proton decay to the ground state of ^{31}P, as may be seen in the coincident spectra in Figs. 18(b) and 18(c) and the resultant branching ratios listed in Table IV. The present results are in qualitative agreement with those of McGrath *et al.*, but the alpha branching ratios are somewhat smaller. This $T=2$ state has been studied[17] as a resonance in the ^{31}P(p,γ) reaction and the ^{31}P(p,p) reaction has been used to set an upper limit of 170 eV for its total width (with the assumption of 100% p_0 branching ratio).

G. ^{36}Ar (10.86 MeV, $T=2$)

The branching ratio for particle decay of the lowest $T=2$ state in ^{36}Ar had not been previously measured. The state was populated by the ^{38}Ar(p,t)^{36}Ar reaction with 42 MeV protons incident on ^{38}Ar gas (isotopically enriched to >95%). The gas cell was a 1 cm diameter cylinder 7 cm long. Tritons passed through a 2 mm diameter exit window covered by a 500 μg/cm^2 Ni foil at 23° to the axis of the gas cell and in line with the en-

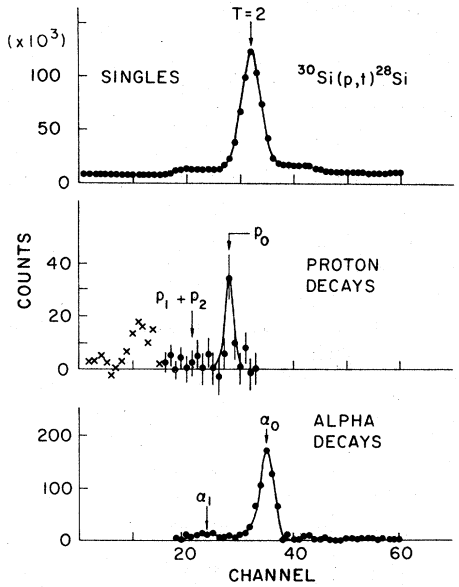

FIG. 17. Singles triton spectrum and coincidence spectra for proton and alpha decays of the ^{28}Si (15.22 MeV, $T=2$) level (see caption of Fig. 14).

trance aperture of the QDDD. Decay particles passed through a 1 cm diameter 625 μg/cm^2 Ni window at −90% viewed by a two-element telescope consisting of a 35- and a 500-μm surface barrier detector. The beam entered through a 2.5 μm Al window covered by 7μg/cm^2 of Formvar and exited through a 4 μm Havar foil. The pressure in the cell was maintained at 50 Torr during the experiment. The overall detection efficiency

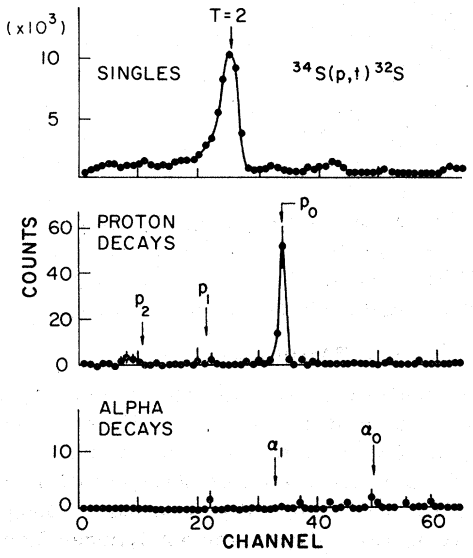

FIG. 18. Singles triton spectrum and coincidence spectra for proton and alpha decays of the ^{32}S (12.05 MeV, $T=2$) level. (See caption of Fig. 14).

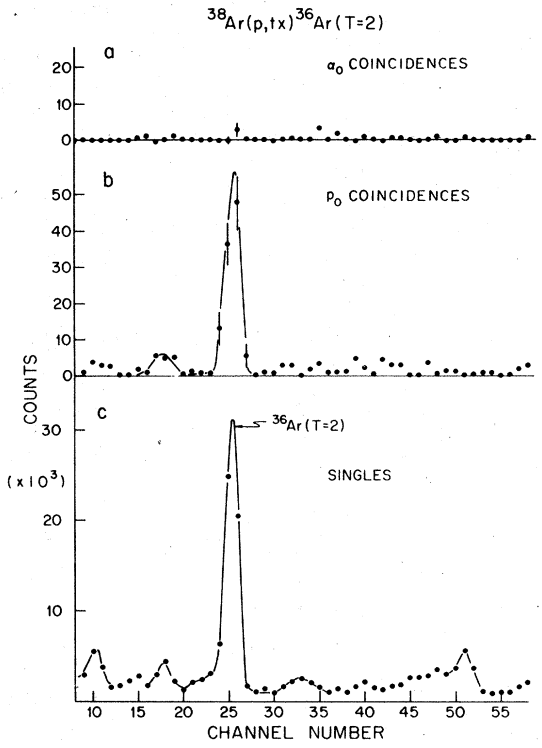

FIG. 19. QDDD focal plane position spectra for identified tritons from the ^{38}Ar$(p,t)^{36}$Ar reaction (c) in singles mode, (b) in coincidence with protons corresponding to decays to the ground state of ^{35}Cl, and (a) in coincidence with α particles corresponding to decays to the ground state of ^{32}S.

was measured as described in Sec. IIB, using the ^{14}N$(p,d)^{13}$N reaction on nitrogen gas.

The $T=2$ state in ^{36}Ar was observed to decay only by proton emission to ^{35}Cl (g.s.) as indicated in Fig. 19 and Table V. The γ-decay properties of this level have been studied[34,35] by the ^{35}Cl(p,γ) reaction but the total width has not been determined. From the experimental resolution in the QDDD the width must be <35 keV.

TABLE V. Branching ratios (%) of lowest $T=2$ levels ($J^\pi=0^+$).

Channel	Present work	Ref. 8
	^{36}Ar(10.86 MeV, $T=2$)	
$\alpha+{}^{32}$S(0_0^+)	<6	...
$p+{}^{35}$Cl$(\frac{3}{2}^+_0)$	109 ± 15	...
$+{}^{35}$Cl$(\frac{1}{2}^+_0)$	<4	
	^{40}Ca(11.98, $T=2$)	
$\alpha+{}^{36}$Ar(0_0^+)	93 ± 9	116 ± 11
$+{}^{36}$Ar(2_0^+)	<3	−1 ± 2
$p+{}^{39}$K$(\frac{3}{2}^+_0)$	<5	−3 ± 9

H. ^{40}Ca (11.98, $T = 2$)

The spectrum of tritons observed at 27° from the ^{42}Ca$(p,t)^{40}$Ca reaction at $E_p = 42$ MeV is shown in Fig. 20. The target consisted of ~200 μg/cm^2 of ^{42}Ca (isotopically enriched to >95%) evaporated on a 20 μg/cm^2 carbon foil and transferred to the target chamber in a vacuum lock. The only significant decay branch observed was alpha decay to the ground state of ^{36}Ar, as may be seen from the coincidence spectra in Fig. 20 and the resultant branching ratios listed in Table V. The present results are in agreement with those of McGrath *et al.*[8] This $T = 2$ state has never been observed as an isospin forbidden resonance. The observed width in the present measurement may be used to define $\Gamma < 20$ keV.

I. ^{44}Ti (9.34 MeV, $T = 2$)

Details of the measurement of branching ratios for alpha and gamma decay of the lowest $T = 2$ level of ^{44}Ti have been given in a previous publication.[23] These results may be combined with a measurement[36] of $\Gamma_\alpha\Gamma_\gamma/\Gamma = 0.24 \pm 0.05$ eV to determine the total and partial widths for this level as listed in Table IV.

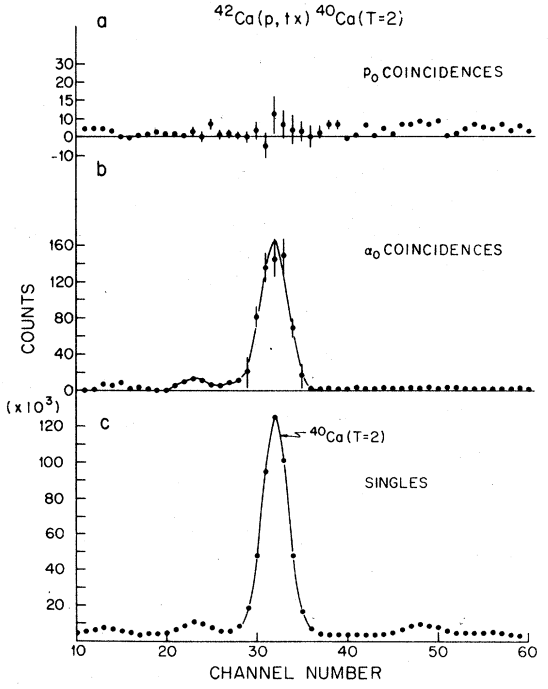

FIG. 20. QDDD focal plane position spectra for identified tritons from the ^{42}Ca$(p,t)^{40}$Ca reaction (c) in singles mode, (a) in coincidence with protons corresponding to decays to the ground state of ^{39}K, and (b) in coincidence with α particles corresponding to decays to the ground state of ^{36}Ar.

IV. DISCUSSION

Very few calculations of isospin forbidden particle decay widths of $T = 2$ levels have been performed. However, for ^{8}Be, where the spectrum and structure of possible admixed levels is particularly simple, Barker and Kumar[37] have been remarkably successful in predicting partial and total decay widths, as may be seen in Table I. They find that the isospin mixing due to the Coulomb interaction is dominated by the third $T = 0$ state which is predominantly the LS coupled $[22]^{11}$S configuration which has a space wave function similar to the $T = 2$ state. The orbital symmetry of this state favors decay by deuteron emission to the ground and first excited states of ^{6}Li and inhibits proton, neutron, and alpha decays to low-lying states. The close agreement in ^{8}Be between the measured decay widths and those calculated from Coulomb mixing alone does not support the conjecture of a significant $\Delta T = 1$ charge dependence of the short range nuclear force which has been invoked[38] to explain the Nolen-Schiffer anomaly.[39] The close agreement for the absolute magnitudes of the widths may be fortuitous, however, since the isospin admixture depends on the relative spacing of the 0^+, $T = 0$ and 0^+, $T = 2$ states, which has not been determined experimentally. In fact, there is evidence[40] from the isobaric multiplet mass equation that the admixing $T = 0$ state may lie below the $T = 2$ state, rather than above, as in Barker's calculation.

The influence of structural symmetry is particularly striking for the α_0 decay, which is sensitive only to the [4] configuration. The decay is highly inhibited with $\theta_\alpha^2 = (0.5 \pm 1.0) \times 10^{-6}$. On the other hand, the orbital symmetry does not inhibit decays to excited states of ^{4}He, and the most impressive feature of the ^{8}Be$(T = 2)$ decays is the relative strength of the branch to the 20.2 MeV 0^+, $T = 0$ state of ^{4}He. This branch has $\theta_\alpha^2 = (54 \pm 9) \times 10^{-6}$, at least a factor of 30 greater than the α_0 branch. Barker[36] did not consider decays to the 20.2 MeV state, since his wave functions contained only an inert 0s shell core. The strength of the α_1 branch presumably arises because the ^{4}He excited state has a [22] configuration to which decays are favored.

The α decays of ^{16}O$(T = 2)$ show an interesting similarity to those of ^{8}Be $(T = 2)$. The α_0 decays are again weak, $\theta_\alpha^2 = (19 \pm 10) \times 10^{-6}$, while decays to the excited 0^+ state of ^{12}C are much stronger, with $\theta_\alpha^2 = (260 \pm 85) \times 10^{-6}$. This presumably again indicates that the Coulomb interaction readily mixes $T_<$ states with (2p – 2h) space configurations, which are similar to those of the $T = 2$ state. This trend may persist in heavier nuclei, since ^{20}Ne

has a strong decay branch to the unresolved 3^- and 0^+ states in ^{16}O at $E_x \sim 6$ MeV.

The available information on partial decay widths for $T=2$ levels is now sufficiently complete that it is appropriate to look for systematic trends with mass number such as were observed for $T=\frac{3}{2}$ levels.[2,3,4] Figures 21 and 22 show the reduced widths, θ^2, for proton and alpha decays of the $T=2$ levels, plotted as a function of mass. Although the present results are generally not as accurate as those for the $T=\frac{3}{2}$ levels (Fig. 23) a number of trends are worth noting.

First, the general magnitudes of the reduced widths, and also their slope as a function of A are quite similar for the decays of the $T=\frac{3}{2}$ and $T=2$ levels. This is further evidence for the regularity of the T-forbidden decays and suggests that we can learn general properties of isospin mixing from such decays.

Second, reduced widths are similar for alpha ($T=0$) and proton ($T=0$ or 1) decay channels indicating that isotensor ($\Delta T=2$) and isovector ($\Delta T=1$) mixing matrix elements are of similar magnitude. This result has recently been discussed[41] in terms of the isospin mixing of $T=0$ and $T=1$ antianalog configurations due to the Coulomb interaction. These mixing matrix elements involve differences of single proton-core and two-proton Coulomb matrix elements which can be derived from Coulomb energy differences, using a simple schematic model for the dominant configurations. Although single proton-core (isovector) Coulomb matrix elements are much larger than two-proton Coulomb matrix elements, the mixing of $T=0$ and $T=1$ anti-analog configurations invariably involves differences of these matrix elements for protons in different valence orbits. These differences are similar in magnitude producing significant isovector and isotensor mixing. The similarity of isovector and isotensor matrix elements also results in significant differences in analogous neutron and proton decay widths for $T=\frac{3}{2}$, $T_z=\pm\frac{1}{2}$ nuclei, as is observed experimentally[3] (see Fig. 23).

More detailed calculations of isospin forbidden decay widths must determine the distribution of $T_<$ levels with appropriate J^π and their allowed decay probability for the various channels. However, the relatively regular variation with mass of the isospin forbidden reduced widths of the $T=2$ and $T=\frac{3}{2}$ levels and their similarity in magnitude, lends credence to the assumption that the mixing may be dominated by some general configuration, such as the antianalog states. For the alpha decays, the reduced widths to excited states are as large as or larger than those to the ground state.

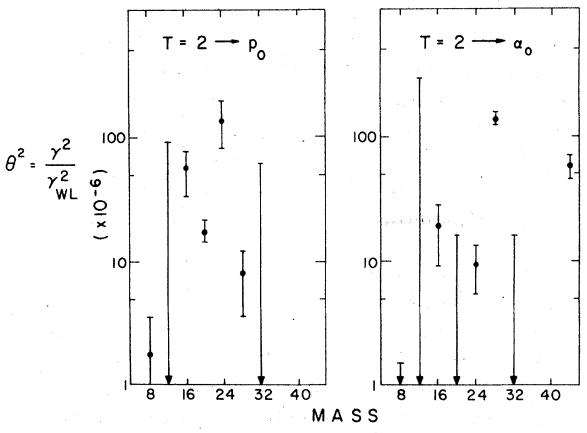

FIG. 21. Reduced widths $\theta^2=\gamma^2/\gamma_{WL}{}^2$ for isospin-forbidden proton (alpha) decays of $A=4N$, $T=2$ levels to the ground state of $A=4N-1$ ($A=4N-4$) nuclei.

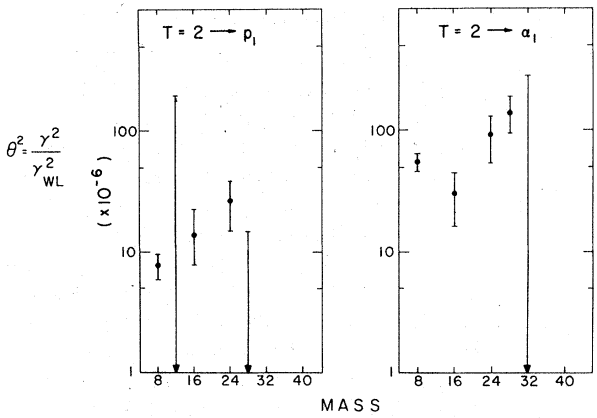

FIG. 22. Reduced widths $\theta^2=\gamma^2/\gamma_{WL}{}^2$ for isospin-forbidden proton (alpha) decays of $A=4N$, $T=2$ levels to the first excited state of $A=4N-1$ ($A=4N-4$) nuclei.

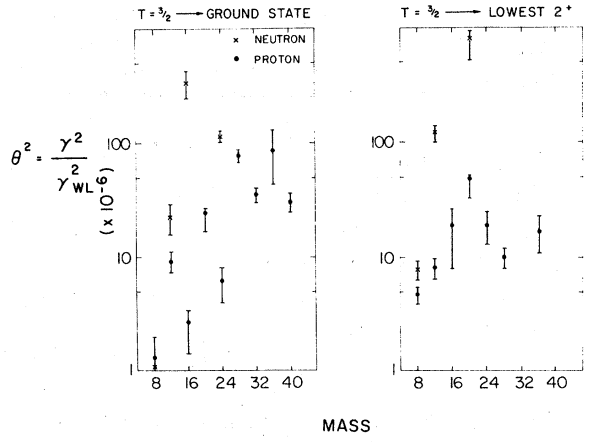

FIG. 23. Reduced widths $\theta^2=\gamma^2/\gamma_{WL}{}^2$ for isospin-forbidden proton (dots) and neutron (crosses) decay of the lowest $T=\frac{3}{2}$ levels of $A=4N+1$ nuclei to the ground state and lowest 2^+ level of $A=4N$ nuclei.

This is compatible with mixing of the antianalog configurations, having 2p – 2h structure similar to the $T=2$ level.

The $\Delta A=8$ periodicity observed for the proton reduced widths of $T=\frac{3}{2}$, $T_z=-\frac{1}{2}$ levels[4] may be observable in the reduced widths for p_0 decay of the $T=2$ levels, but is not evident in the α_0 or α_1 widths. This is similar to the $T=\frac{3}{2}$ case where the oscillation is not observed in the reduced widths for proton decay to the lowest 2^+ levels, or in neutron decays from $T=\frac{3}{2}$, $T_z=+\frac{1}{2}$ levels to ground states or excited states. This suggests that the oscillation is not representative of an overall variation in isospin impurity amplitudes, but is dependent both on isospin mixing and decay probabilities to the particular channels involved.

Further improvements in the accuracy of isospin forbidden particle decay widths of $T=2$ levels must come primarily from resonance studies. It is interesting to predict total widths for the presently unobserved cases assuming reduced widths similar to those in Figs. 21 and 22.

For ^{12}C if θ^2 (p_0 or α_0) $\approx 10\times10^{-6}$, then $\Gamma\approx 6$ or 1 keV, respectively. However, a total width of 30 keV would be consistent with the neighboring reduced widths. For ^{36}Ar, θ^2 (p_0) $\lesssim 50\times10^{-6}$ implies $\Gamma\lesssim 6$ eV and for ^{40}Ca, $\theta^2(\alpha_0)\lesssim 50\times10^{-6}$ implies $\Gamma\lesssim 7$ eV. These widths are small enough that gamma branching ratios may be measurable. (For ^{36}Ar, $\Gamma_{M1}=0.08\pm0.02$ eV).

Although such experiments to determine the widths of $T=2$ states with $A\leq 36$ are difficult, they are definitely worth pursuing in order to see if the completely unexplained $\Delta A=8$ oscillations seen in p_0 decay widths of $T=\frac{3}{2}$ states are present in decays of the $T=2$ states as well.

In summary, the information now available on isospin-forbidden particle decay widths of $T=\frac{3}{2}$ and $T=2$ levels in light nuclei indicates relatively regular trends as a function of mass. This suggests the dominance of a general isospin-mixing mechanism. Relatively large isotensor mixing is observed, which might be thought to arise from a charge dependent nuclear interaction. However, a simple model indicates[41] that such isotensor matrix elements can arise from the Coulomb interaction so that the identification of specifically nuclear charge-dependent effects in particle decay widths will be very difficult, and will require detailed nuclear structure calculations for each case.

---

*Present address: Department of Physics, Stanford University, Stanford, California 94305.
†Present address: LAMPF, Los Alamos Scientific Lab., Los Alamos, N. M. 87545.
‡Present address: Lawrence Berkeley Laboratory, University of California, Berkeley, California 94720.
§Present address: Department of Physics, Michigan State University, East Lansing, Michigan 48824.

[1]E. G. Adelberger, A. B. McDonald, C. L. Cooke, C. N. Davids, A. P. Shukla, H. B. Mak, and D. Ashery, Phys. Rev. C7, 889 (1973).
[2]E. G. Adelberger, in *Proceedings of the International Conference on Nuclear Structure and Spectroscopy, Amsterdam*, edited by H. P. Blok and A. E. L. Dieperink (Scholar's Press, Amsterdam, 1974), p. 641.
[3]A. B. McDonald, H. B. Mak, H. C. Evans, G. T. Ewan, and H. B. Trautvetter, Nucl. Phys. A273, 477 (1976) and references therein.
[4]P. G. Ikossi, W. J. Thompson, T. B. Clegg, W. W. Jacobs, and E. J. Ludwig, Nucl. Phys. A274, 1 (1976).
[5]A. B. McDonald, T. K. Alexander, and O. Hausser, Nucl. Phys. A37, 545 (1969).
[6]H. Weigmann, R. L. Macklin, and J. A. Harvey, Phys. Rev. C14, 1328 (1976).
[7]T. K. Koh, W. R. Falk, N. E. Davison, and J. M. Nelson, Phys. Rev. C7, 50 (1973).
[8]R. L. McGrath, J. Cerny, J. C. Hardy, G. Goth, and A. Arima, Phys. Rev. C1, 184 (1971).
[9]J. L. Black, W. J. Caelli, D. L. Livesey, and R. B. Watson, Phys. Lett. 30B, 100 (1969).
[10]J. W. Noé, D. F. Geesaman, P. Paul, and M. Suffert, Phys. Lett. 65B, 125 (1976).
[11]A. V. Nero, R. E. Pixley, and E. G. Adelberger, Phys. Rev. C6, 679 (1972).
[12]R. Block, R. G. Pixley, and P. Truol, Phys. Lett. 25B, 215 (1967).
[13]H. M. Kuan *et al.*, Phys. Lett. 25B, 217 (1967).
[14]F. Reiss, W. J. O'Connell, D. W. Heikkinen, H. M. Kuan, and S. S. Hanna, Phys. Rev. Lett. 19, 307 (1967).
[15]N. A. Jelley, N. Anyas-Weiss, M. R. Wormald, B. T. Underwood, and K. W. Allen, Phys. Lett. 40B, 200 (1972).
[16]D. P. Balamuth and E. G. Adelberger, Phys. Rev. C16, 928 (1977).
[17]J. Vernotte, S. Gales, M. Langevin, and J. M. Maison, Phys. Rev. C8, 178 (1973).
[18]W. R. Dixon, R. S. Storey, J. J. Simpson, and R. D. Lawson, Phys. Rev. C13, 1745 (1976).
[19]A. B. McDonald, E. D. Earle, W. McLatchie, H. B. Mak, D. Martin, and P. G Ikossi, Nucl. Phys. A305, 151 (1978).
[20]J. L. Osborne, E. G. Adelberger, and K. A. Snover, Nucl. Phys. A305, 144 (1978).
[21]P. G. Ikossi, K. A. Snover, J. L. Osborne, E. G. Adelberger, and A. B. McDonald, Bull. Am. Phys. Soc. 23, 521 (1978); and (to be published).
[22]J. B. Marion and F. C. Young, *Nuclear Reaction Analysis* (North-Holland, Amsterdam, 1968).
[23]S. J. Freedman, C. A. Gagliardi, M. A. Oothoudt, A. V. Nero, R. G. H. Robertson, F. J. Zutavern, E. G. Adelberger, and A. B. McDonald, Phys. Rev. C17, 2071 (1978).
[24]V. V. Verbinskii, W. R. Burrus, T. A. Love, W. Zobel, and N. W. Hill, Nucl. Instrum. Methods 65, 8 (1968).
[25]F. Hinterberger, P. V. Rossen, E. Lebsanft, P. Lütticken, J. Bisping, R. Jahn, and B. Schüller, Nucl. Phys. A259, 385 (1976).

[26]D. Ashery, M. S. Zisman, G. W. Goth, G. J. Wosniak, R. B. Weisenmiller, and J. Cerny, Phys. Rev. C13, 1345 (1976).
[27]K. A. Snover, Ph.D. thesis, Stanford University, 1969 (unpublished).
[28]J. L. Black, W. J. Caelli, and R. B. Watson, Phys. Rev. Lett. 25, 877 (1970).
[29]E. K. Warburton, H. M. Kuan, D. E. Alberger, P. Paul, and K. A. Snover, Phys. Rev. C6, 375 (1972).
[30]S. S. Hanna, M. Hass, Z. Shkedi, and Y. S. Horowitz, Nucl. Phys. A195, 91 (1972).
[31]R. G. H. Robertson, T. L. Khoo, G. M. Crawley, A. B. McDonald, E. G. Adelberger, and S. J. Freedman, Phys. Rev. C17, 1535 (1978).
[32]A. B. McDonald, P. G. Ikossi, H. B. Mak, D. Martin, and E. D. Earle, unpublished.
[33]J. Szücs, B. Y. Underwood, T. K. Alexander, and N. Anyas-Weiss, Nucl. Phys. A212, 293 (1973).
[34]D. J. Martin, H. C. Evans, and J. A. Szücs, Phys. Rev. C14, 1320 (1976).
[35]A. Huck, G. J. Costa, G. Walter, M. M. Aleonard, J. Dalmas, P. Hubert, F. Lecuo, P. Mennrath, J. Vernotte, M. Langevin, and J. M. Maison, Phys. Rev. C13, 1786 (1976).
[36]J. L. Simpson, W. R. Dixon, and R. S. Storey, Phys. Rev. Lett. 29, 1472 (1972); W. R. Dixon, R. S. Storey, J. J. Simpson, and R. D. Lawson, Phys. Rev. C13, 1945 (1976).
[37]F. C. Barker and N. Kumar, Phys. Lett. 30B, 103 (1969).
[38]J. W. Negele, in *Proceedings of the International Conference on Nuclear Structure and Spectroscopy, Amsterdam*, edited by H. P. Blok and A. E. L. Dieperink (Scholar's Press, Amsterdam, 1974).
[39]J. A. Nolan Jr. and J. P. Schiffer, Annu. Rev. Nucl. Sci. 19, 471 (1969).
[40]R. G. H. Robertson, W. Benenson, E. Kashy, and D. Mueller, Phys. Rev. C13, 1018 (1976); R. G. H. Robertson, E. Kashy, W. Benenson, and A. Ledebuhr, *ibid.* 17, 4 (1978).
[41]A. B. McDonald and E. G. Adelberger, Phys. Rev. Lett. 40, 1692 (1978).